17

Two Intersecting Internal Wave Rays: A Comparison Between Numerical and Laboratory Results

A. Javam, S. G. Teoh, J. Imberger and G. N. Ivey

Abstract

The interaction between two downward propagating internal wave rays in a linearly stratified fluid was examined numerically and experimentally. The numerical simulations employed a SIMPLE scheme with a third order QUICK discretization for the advective terms and second order Crank-Nicholson scheme on a non-staggered grid to solve the full unsteady equations of motion in an open domain with boundary conditions based on the Sommerfield radiation condition. The laboratory experiments were performed in a glass-walled tank filled with a linearly stratified salt solution with two identical wave paddles used to generate two internal wave rays. The interaction between the two wave rays was visualized by bull eye's rainbow schlieren and shadowgraph techniques, in conjunction with velocity measurements made by particle image velocimetry. Good agreement was found between the observed and simulated interaction mechanisms. The nonlinear nonresonant interaction of two wave rays with identical properties, but opposite horizontal phase velocities, led initially to the formation of small spatial scales followed by the development of evanescent modes. The evanescent modes, with frequencies greater than the local buoyancy frequency, were trapped within the intersection region. The energy transferred to the trapped evanescent modes ultimately causing overturning of the density field in the intersection region.

Introduction

Internal waves play an important role in the distribution of the momentum and energy throughout stratified water bodies (Thorpe, 1975; Imberger, 1994) and provide a linkage between the energy-containing scales and the dissipative scales (Munk, 1981; Muller et al., 1991; Imberger, 1994). Therefore, an understanding and parameterization of these transfer, mixing and dissipation processes are essential for a description of the circulation and transport in stratified water bodies.

Resonant triad interaction is believed to be a significant mechanism in energy transfer to other modes. As a result, this mechanism has been widely investigated (e.g. Hasselmann, 1966; Bretherton, 1964; Phillips, 1960; Thorpe, 1966, 1987a, 1987b; Davis and Acrivos, 1967; Simmons, 1969; Martin et al., 1972; McComas and Bretherton, 1977;

Physical Processes in Lakes and Oceans
Coastal and Estuarine Studies Volume 54, Pages 241-250

Thorpe, 1987b). Triad interaction among internal waves redistributes energy and momentum among different wave components. Resonant interactions may also cause the amplitude of parasitic waves to grow once the amplitude of host waves exceeds a critical value (McEwan, 1971). Eventually, an instability occurs and the ambient stratified water is mixed (McEwan, 1971, 1983a, 1983b; Taylor, 1992).

Wave energy can be transferred towards frequencies lower than the forcing frequency (Martin et al., 1969, 1972; McEwan, 1971; McEwan and Robinson, 1975). Any resonant triad consisting of a finite amplitude wave and two infinitesimal components is unstable for the sum interaction and neutrally stable for the difference interaction (Hasselmann, 1967; McEwan, 1971). Note that each of the three waves participating in a resonant triad is an exact solution of the equation of motion (within the inviscid and Boussinesq approximations).

Nonlinear nonresonant interactions have received comparatively little attention, even though they also transfer energy across the spectrum. McEwan (1973) studied the nonlinear nonresonant interactions between two rays and showed that the Richardson, number was large before the occurrence of 'traumata'; isopycnal slopes were, however greater than 30°. Thorpe (1987a) illustrated that second order resonance between an incident and a reflected wave from a slope only occurs when the slope and the incident ray are less than 8.4° and 30°, respectively, to the horizontal. The evanescent modes can be excited by the effects of nonlinearity (Thorpe, 1987b; Ivey et al, 1995). The excited evanescent modes play a crucial role in producing density overturning. In this paper it will be shown both experimentally and numerically that two intersecting beams of internal waves do become unstable, not by resonant triad interaction, but rather by transferring energy to standing evanescent modes, ultimately leading to overturning of the density field.

Laboratory and Numerical Models

Laboratory Model

A schematic of the experimental configuration is shown in Figure 1. The experimental glass-walled tank of length 5900 mm, depth 540 mm and width 535 mm, was filled with linearly stratified salt solution, using the standard two-tank system. Two identical wave-paddles, each consisting of eight blades which could pivot independently about their long central axes, were used to generate internal wave rays. The wave paddles were separated, centre to centre, by 615 mm and located horizontally near the centre of the tank, 40 mm below the free surface. Only the central six blades were oscillated, forming either an M or W shape, and internal waves rays of width 1.5 times the wavelength were generated. The central amplitude of each paddle was twice that at both sides of the paddle to minimise the net volume flux induced by blade displacements.

Flow visualisation inside the intersection region was achieved by rainbow colour schlieren (Howes, 1984; Ivey & Nokes, 1989) and shadowgraph (Merzkirch, 1974). The evolution of the density field was complemented by time series of density and profiles obtained with conductivity and temperature measurements. Digital particle image velocimetry (DPIV) was used to complement the results from flow visualisation (Stevens & Coates, 1994). A detailed description of the experimental configuration is given in Teoh et al. (1997).

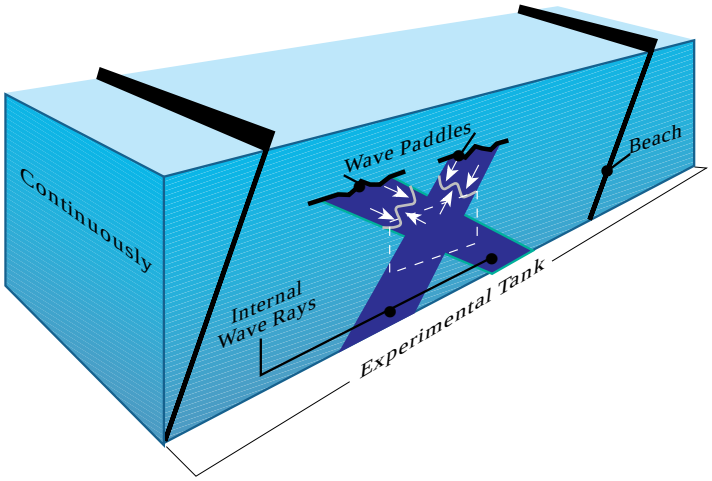

Figure 1. Schematic of the experimental tank.

Numerical Model

The conservation of momentum, mass and volume are expressed in non-dimensional form in Euclidean coordinates, (x, y) with corresponding velocity components (u, v) as follows,

$$\frac{\partial u}{\partial t} + \mathrm{Fr}\left[u\frac{\partial u}{\partial x} + v\frac{\partial u}{\partial y}\right] = -\frac{\partial p}{\partial x} + \mathrm{Re}^{-1}\nabla^2 u, \tag{1}$$

$$\frac{\partial v}{\partial t} + \mathrm{Fr}\left[u\frac{\partial v}{\partial x} + v\frac{\partial v}{\partial y}\right] = -\frac{\partial p}{\partial y} - \rho + \mathrm{Re}{-}1\nabla 2v + \sin(t)\big(f_1,(x,y) + f_2(x,y)\big), \tag{2}$$

$$\frac{\partial \rho}{\partial t} + \mathrm{Fr}\left[u\frac{\partial \rho}{\partial x} + v\frac{\partial \rho}{\partial y}\right] = \mathrm{Ri}\, v + \mathrm{Re}^{-1}\,\mathrm{Pr}^{-1}\nabla^2\rho, \tag{3}$$

$$\frac{\partial u}{\partial x} + \frac{\partial v}{\partial y} = 0, \tag{4}$$

$$\mathrm{Ri} = \frac{(-g/\rho_0)(d\hat{\rho}/dy)}{\omega^2} = \left[\frac{N}{\omega}\right]^2, \tag{5}$$

$$\mathrm{Fr} = \frac{F}{L\omega^2}, \tag{6}$$

$$\mathrm{Pr} = \frac{v}{\kappa}, \tag{7}$$

$$\mathrm{Re} = \frac{L^2\omega}{v}, \tag{8}$$

$$\nabla^2 = \frac{\partial^2}{\partial x^2} + \frac{\partial^2}{\partial y^2},$$

and where $N = (g/\rho_0 (d\hat{\rho}/dy))^{1/2}$ is the buoyancy frequency, t is the time, ρ, $\hat{\rho}$ and ρ_0 are the fluctuating, background and reference densities, respectively, ν is the coefficient of kinematic viscosity, κ is the diffusivity, $f_1(x,y)$ sin t and f_2 (x, y) sin t are the momentum sources used to generate two internal wave beams, ω is the frequency of the momentum sources, $f_1(x,y)$ and $f_2(x,y)$ are the dimensionless localization functions, F is the amplitude of the momentum source, and L is the scale of the standing wavelike momentum source. The localization functions $f_i(x,y)$ are given by:

$$f_i(x,y) = \begin{cases} \cos(2\pi x_1)\exp(-300\,|\,y_1\,|^3) & \text{if } |\,x_1\,| \leq 0.5 \\ \left[\cos(2\pi x_1)\exp(-300\,|\,y_1\,|^3)\right]/2 & \text{if } 0.5 < |\,x_1\,| \leq 0.75 \\ 0.0 & \text{otherwise} \end{cases} \tag{9}$$

in which x_l and y_l are the horizontal and vertical dimensionless distances from the location of the momentum source.

The equations of motion (1)–(4) were solved by the SIMPLE scheme (Patankar, 1980) with a QUICK correction for the convection terms (Leonard, 1979) on a non-staggered grid using a finite volume method (Armfield, 1994). In order to ensure that waves continue to propagate unchanged through the boundaries, an open boundary condition, based on the Sommerfield radiation condition, was formulated. A detailed description of the numerical method, the discrete equations and open boundary conditions is given in Javam et al. (1997a).

Comparison between Numerics and Experiments

To investigate the wave-wave interaction, the spatial domain was discretized with 240 $\times$ 160 uniform cells with the nondimensional mesh size of $\Delta x = \Delta y = 0.05$. The two momentum sources were located at ($0.35L_x$, $0.50L_y$) and ($0.65L_x$, $0.50L_y$) where L_x and L_y are the length and width of the computational domain, respectively (Figure 2). Velocity vector plots are shown in Figure 2 for the case: Fr = 0.1, Ri = 2.5, Re = 25,000 and Pr = 700, ten wave periods after start up from rest. The rays generated by the momentum sources travelled away from the sources and the wave energy was transported along the ray path or direction of the group velocity vector. The wave number vectors were normal to the group velocity vectors and were directed to the horizontal. The rays intersected in two regions called interaction regions (Figure 2); we will only present the results from the lower interaction region for comparison with the experiments.

In the laboratory experiment, the dimensional scales were: L = 191 mm, N = 1 r/s, ω = 0.4 r/s and salt was used to stratify the fluid. In the numerical model this choice resulted in Re = 15000, Ri = 6.25 and Pr = 700. In order to have a similar wave field between numerical and experimental study, we set the Froude number Fr to 0.75 which resulted in the same wave amplitude within the rays in both the experiments and the numerics.

Figure 3 shows a comparison between a schlieren image from the laboratory experiment and density gradient contours from the numerical model in the intersection region. The schlieren images were sensitive to the changes in the first derivitive of the density field (Howes, 1984). Within the intersection, the wave induced density gradient

fluctuations grew and eventually developed a regular pattern propagating vertically upwards as shown in Figure 3. The density gradient fluctuations in Figure 3 were symmetric about the vertical axis. The schlieren images from the experiment (Teoh et al., 97) show the appearance of a new mode and later a turbulent patch along the horizontal axis near the centre of the image. A black colour region was observed to surround this patch indicating a strong density gradient boundary. New rays generated by turbulent fluctuations were subsequently seen to radiate outwards from a point above the patch.

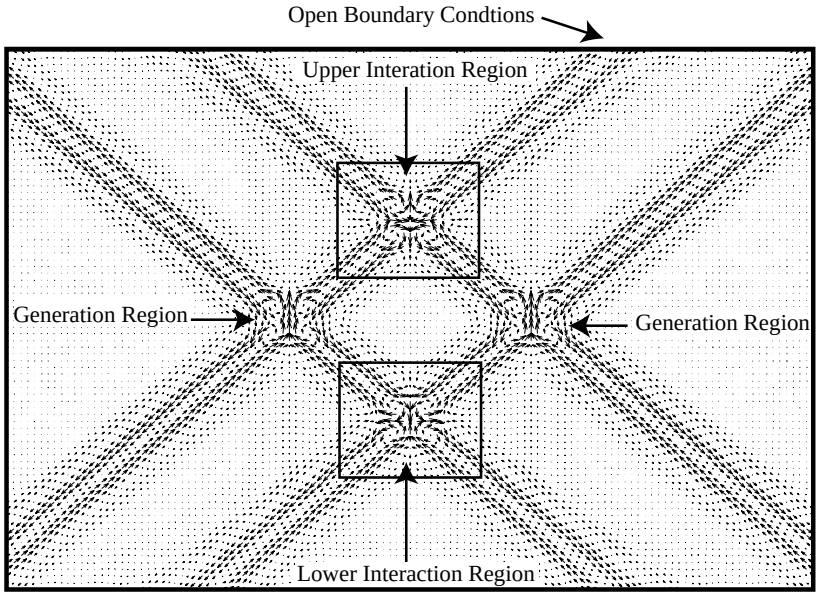

Figure 2. Velocity vector plots for the internal wave, Ri = 2.5, Fr = 0.1, Pr = 700 and Re = 25000; at time T=10. Two momentum sources are used to generate internal waves.

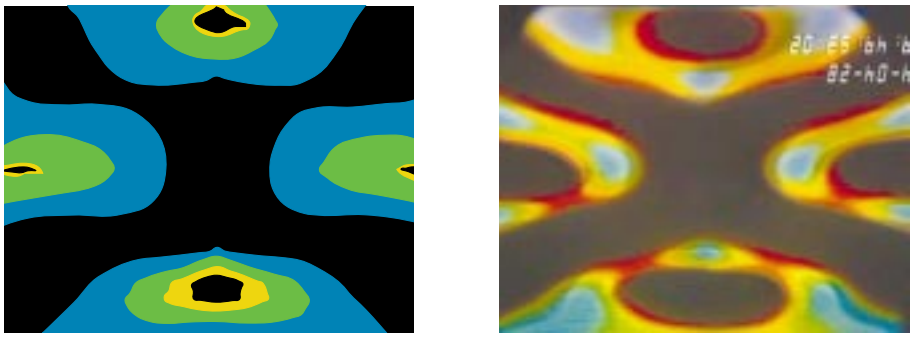

Figure 3. Rainbow colour Schlieren picture (on the right) and density gradient contours from the numerics.

The corresponding velocity field is shown in Figure 4. The velocity field exhibits stagnation points propagating vertically upwards within the intersection region. Horizontal compression and dilation straining are visible at the stagnation points, demonstrating that a fluid volume centred around a fixed point on the centreline of the interaction region is successively compressed and dilated.

Density profiles, at one wave period apart, illustrating the effect of this forcing in the progression towards gravitationally unstable overturning from T = 4.3 to T = 10.3 are shown in Figure 5a. The density profile at T = 8.3 in the numerical model shows the presence of the primary resultant wave and the locally produced new modes which had

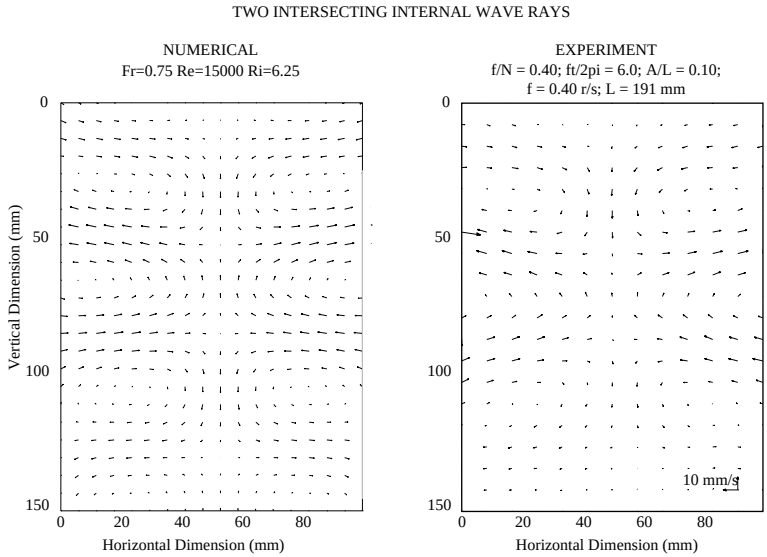

Figure 4. Velocity vector plots. Horizontal compressive and dilation straining visible at the stagnation points.

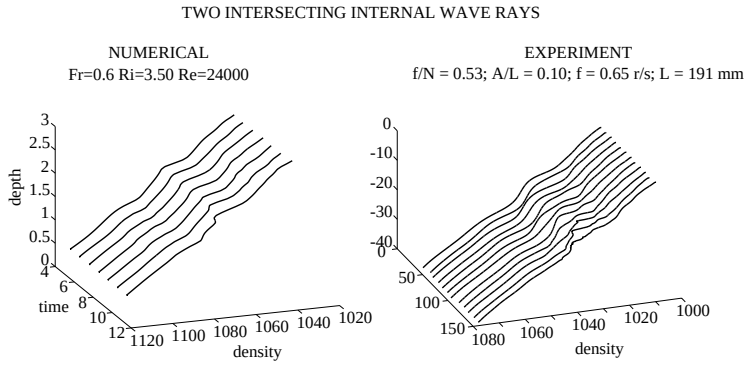

Figure 5. Vertical profiles of density for numerical and experimental results. New modes with the shorter vertical wavelengths are produced.

shorter vertical wavelengths. The result from the laboratory experiment shows a similar feature to the numerical model but shows much smaller scales which can not be resolved by the numerical model due to the restriction in mesh sizes.

The density fluctuation spectra within an incoming ray, an outgoing ray, and within the intersection region illustrate the production of new modes by nonlinear nonresonant interactions between the two rays (Figure 6). Comparison between spectra for incoming and out-going rays (Figures 6a, b) shows that most of the incoming energy was trapped within the interaction region and this trapped energy excited higher modes (Figures 6a,b and c). In the laboratory experiments the central amplitudes of the wave-paddles were twice those at both sides of the paddles; consequently, the wave amplitude varied across the rays. Because of the strong spatial variation in wave amplitude and the difficulty in precisely locating sensors, the result from the experiment can not be directly compared with the numerics (Figures 7a, b). The laboratory experiments were also run for six periods longer than the numerical model and therefore, a number of higher (evanescent) modes were developed which are clearly visible in Figure 7c.

Figures 6 and 7 also show that the level of the spectral energy inside the interaction region was much higher than that of the incoming ray, which implies that the energy was trapped in the interaction region. The density fluctuation spectra within the interaction region (Figures 6 and 7) indicate that the excited modes are multiples of the primary frequency ω. The new modes with frequencies greater than the local buoyancy frequency are thus evanescent modes and cannot propagate (LeBlond and Mysak, 1978). Therefore the energy transfer from ω to the evanescent modes provides a mechanism to accumulate energy locally and subsequently leading to overturning as seen in Figure 5b for longer times.

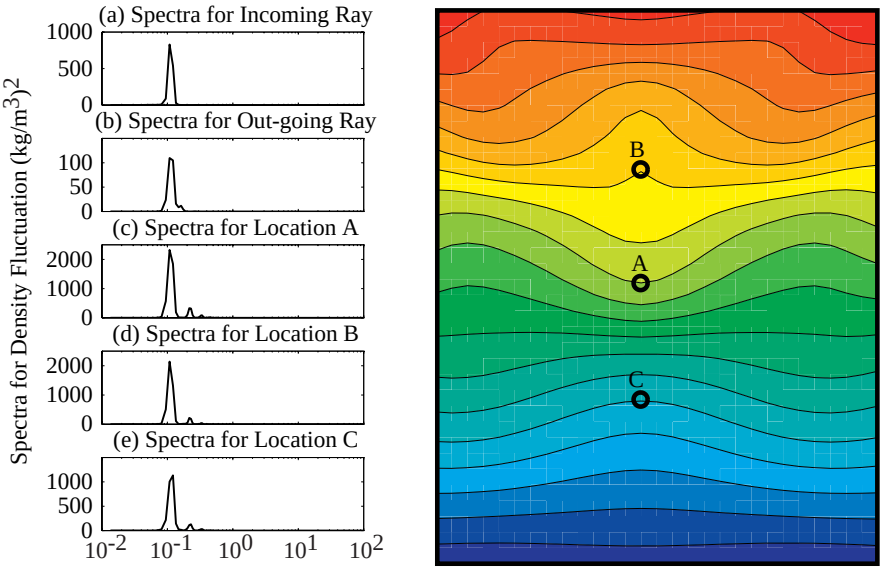

Figure 6. Spectra for density fluctuations from the numerical simulation: Ri = 2, Fr = 0.375, Pr = 7 and Re = 25000. The trapped energy excites higher modes.

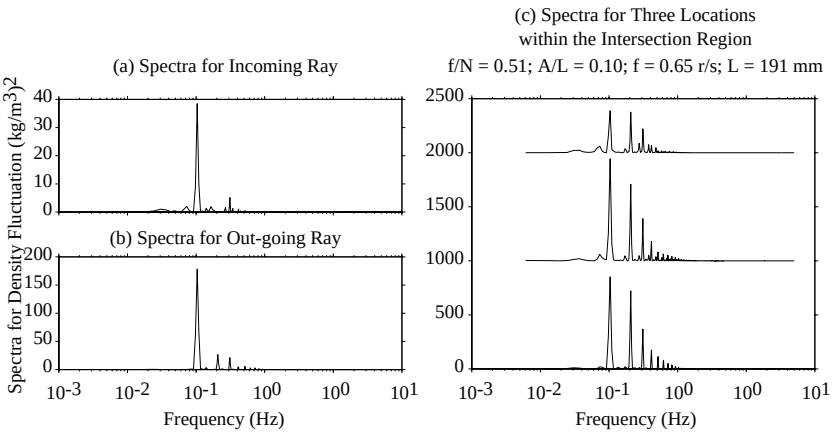

Figure 7. Spectra for density fluctuations from the laboratory experiments Higher modes are excited.

Conclusion

We have presented the results from a combined numerical and experimental study of the nonlinear interaction of internal waves. Both numerical and experimental results showed that nonlinear nonresonant wave-wave interactions transfer wave energy to higher harmonics. Higher harmonics with frequencies greater than buoyancy frequency cannot propagate out of the interaction region. This increases the local energy density within the region which in turn leads to turbulence and mixing. This mechanism of energy transfer towards higher frequencies is similar to either nonlinear interactions between an incident and a reflected wave above a sloping boundary (Thorpe, 1987a; DeSilva, et al, 1997; Javam et al., 1998d) or to interactions near a turning point of a ray propagating against a steady shear (Javam et al, 1997b).

In the numerical experiments the overall energetics and turbulence dynamics could be investigated in detail and the effects of key physical and nondimensional quantities studied via both flow visualisation and parameterization (see Javam et al, 1997b). However, they were restricted by the mesh sizes which can be used whereas the laboratory experiments allowed somewhat smaller scales to be documented as well as the assessment of any three dimensional motions. The above comparison clearly showed that the motions were two dimensional for all scales up to the point where the overturning led to active small scale turbulence.

Acknowledgments. We wish to thank the Centre for Environmental Fluid Dynamics (CEFD) for providing extensive computer resources and for financial support, and also the Hydraulics and Geophysical Fluid Dynamics (GFD) group for providing laboratory equipment.

References

Armfield, S. W., Ellipticity, accuracy and convergence of the discrete Navier-Stokes equations *J. Comput. Phys. Fluids, 114*, 176-184, 1994.

Bretherton, F. P., Resonant interactions between waves: The case of discrete oscillations. *J. Fluid Mech. 20*, 457-479, 1964.

Davis, R. E. and A. Acrivos, Solitary internal waves in deep water. *J. Fluid Mech. 29*, 593-607, 1967.
DeSilva, I. P. D., J. Imberger, and G. N. Ivey, Localised mixing due to a breaking internal wave ray at a sloping bed. *J. Fluid Mech., 350*. 1-27, 1997.
Hasselmann, K., Feyman diagrams and interaction rules of wave-wave scattering processes. *Rev. Geophys. 4*, 1-32, 1966.
Howes, W. L., Rainbow schlieren and its application. *Applied Optics 23*, 2449-2460, 1984.
Imberger, J., Transport processes in lakes: A review article, in *Limnology Now: A Paradigm Of Planetary Problems*, edited by R.. Margalef, pp 99-193, 1994.
Ivey, G. N. and R. I. Nokes, Vertical mixing due to the breaking of critical internal waves on sloping boundaries. *J. Fluid Mech. 204*, 479-500, 1989.
Ivey, G. N., I. D. P. DeSilva, and J. Imberger, Internal waves, bottom slopes and boundary mixing. In *Proceedings 'Aha Huliko' a Hawaiian Winter workshop*, University of Hawaii, pp 199-206, 1995.
Javam, A., J. Imberger, and S. W. Armfield, Numerical study of internal wave-wave interaction. *J. Fluid Mech*. submitted, 1997a.
Javam, A., J. Imberger, and S. W. Armfield, Numerical study of internal wave-shear interactions. *J. Fluid Mech*. submitted, 1997b.
Javam, A., J. Imberger, and S. W. Armfield, Numerical study of internal wave breaking on sloping boundaries. *J. Fluid Mech.* Submitted, 1998.
Martin, S., W. F. Simmons, and C. I. Wunsch, Resonant internal wave interactions. *Nature 224*, 1014-1016, 1969.
Martin, S., W. F. Simmons, and C. I. Wunsch, The excitation of resonant triads by single internal waves. *J. Fluid. Mech. 53*, 17-44, 1972.
McComas, C. H. and F. P. Bretherton, Resonant interaction of oceanic internal waves. *J. Geophys. Res. 82*, 1397-1412, 1977.
McEwan, A. D. and R. M. Robinson, Parametric instability of internal gravity waves. *J. Fluid. Mech. 67*, 667-687, 1975.
McEwan, A. D., Degeneration of resonantly-excited standing internal gravity waves. *J. Fluid. Mech. 50*, 431-448, 1971.
McEwan, A. D., The kinematics of stratified mixing through internal wavebreaking. *J. Fluid. Mech. 128*, 47-57, 1983a.
McEwan, A. D., Internal mixing in stratified fluids. *J. Fluid. Mech. 128*, 59-80, 1983b.
Merzkirch, W., *Flow Visualization*. Academic Press, 1974.
Moller, P., E. A. D'Asaro and G. Holloway, Internal gravity waves and mixing, *in Proceedings 'Aha Huliko' a Hawaiian winter workshop* edited by P. Muller and D. Robinson, pp 499-508, 1991.
Munk, W. H., Internal waves and small scale process. In *Evolution of Physical Oceanography*, edited by B. A. Warren and C. Wunsch, pp. 264-291 Mussachusetts Institute of Technology Press, Cambridge, 1980.
Phillips, O. M., On the dynamics of unsteady gravity waves of finite amplitude. Part I. *J. Fluid Mech. 9*, 193-217, 1960.
Simmons, W. F., A variational method for weak resonant wave interactions. *Proc. Roy. Soc. A. 309*, 551-575, 1969.
Taylor, J. R., The energetics of breaking events in a resonantly forced internal wave field. *J. Fluid Mech. 239*, 304-340, 1992.
Teoh, S. G., G. N. Ivey and J. Imberger, Experimental study of two intersecting internal waves. *J. Fluid Mech. 336*, 91-122, 1997.
Thorpe, S. A., On wave interactions in a stratified fluid. *J. Fluid Mech. 24*, 737-751, 1966.
Thorpe, S. A., The excitation, dissipation, and interaction of internal waves in the deep ocean. *J. Geophys. Res. 80*, 328 338, 1975.
Thorpe, S. A., On the reflection of a train of finite-amplitude internal waves from uniform slope. *J. Fluid Mech. 178*, 279-302, 1987a.
Thorpe, S. A., Transitional phenomena and the development of turbulence in stratified fluids: A review. *J. Geophys. Res. 92*, 5231-5248, 1987b.